Multiple band interactions in ^{131}Nd

D. J. Hartley, W. Reviol,* L. L. Riedinger, D. L. Balabanski,† H. Q. Jin,‡ B. H. Smith,§ O. Zeidan, and Jing-ye Zhang
Department of Physics and Astronomy, University of Tennessee, Knoxville, Tennessee 37996

A. Galindo-Uribarri
Physics Division, Oak Ridge National Laboratory, Oak Ridge, Tennessee 37831

D. G. Sarantites, D. R. LaFosse,‖ and J. N. Wilson¶
Chemistry Department, Washington University, St. Louis, Missouri 63130

S. M. Mullins
Department of Nuclear Physics, Australian National University, Canberra, ACT 0200, Australia
(Received 6 December 1999; published 22 March 2000)

High-spin states in ^{131}Nd were populated in the reaction ^{94}Mo(^{40}Ca,$2pn$) at a beam energy of 180 MeV. Over 170 new transitions were placed in a level scheme that consists of seven rotational structures. The bands were given configuration assignments based on their $B(M1)/B(E2)$ ratios (for the strongly coupled bands), aligned angular momentum, observed band crossings, and signature splitting. Several quasiparticle alignments were observed in the bands and compared with predictions from the cranked shell model. Three-band mixing calculations were performed in order to interpret the low-spin interaction observed in the [411]1/2 band. An examination of the signature splitting for the [541]1/2 bands in ^{129,131,133}Nd revealed information regarding the parentage of the orbital as well as a signature inversion at higher spin.

PACS number(s): 21.10.Re, 23.20.Lv, 27.60.+j

I. INTRODUCTION

The neutron deficient nuclei in the mass 130 region have exhibited a propensity to possess a variety of nuclear shapes. Highly deformed structures (having a quadrupole deformation parameter of $\beta_2 \approx 0.3$–0.4) are well known throughout the region spanning in the ranges $Z=58$–62 and $N=71$–77 (see, for example, Refs. [1–6]). The occupation of a quasineutron in the $\nu i_{13/2}[660]1/2$ orbital [7] and the presence of a hole in the $\pi g_{9/2}[404]9/2$ orbital [8] are often cited as the primary elements for producing bands of large deformation as compared with bands of normal deformation ($\beta_2 \approx 0.22$). Recently, quadrupole moment measurements have proved that structures of ''intermediate'' deformation exist, i.e., having β_2 values of ~ 0.25, which involve the $h_{9/2}/f_{7/2}[541]1/2$ neutron [9–11]. In addition, $A \approx 130$ nuclei are thought to be soft to triaxial deformation [12,13] and bands based upon the $\nu h_{11/2}$ high-K orbitals have particularly shown evidence for nonaxial shapes [14].

An experiment was performed with the high resolving power of Gammasphere [15] for γ-ray detection and the selectivity of the Microball [16] charged particle array to investigate neutron deficient nuclei near $Z=59$ and $A=130$. The emphasis of the experiment was to find new highly deformed bands in the region. For the Nd ($Z=60$) nuclei, these bands are likely based on at least one neutron occupying the intruder [660]1/2 orbital. Structures based on the $\nu i_{13/2}$ orbital have been observed in ^{133,135,137}Nd [14,17,18]; however, as the neutron Fermi surface is lowered from $N=73$, it is increasingly unlikely to observe the [660]1/2 band. In a previous publication [19] resulting from this experiment, evidence was reported for the identification of the [660]1/2 sequence in ^{131}Nd and it was found to have an adiabatic crossing [20] with one of the initially normal deformed bands ([411]1/2). The deformation and configuration differences between normal and highly deformed structures make such a crossing quite rare. In Ref. [19], we raised the possibility that the [411]1/2 band is actually crossed by a ''more-deformed'' band at a frequency just below the crossing with the $\nu i_{13/2}$ structure. The more-deformed band would likely have intermediate deformation and an underlying structure similar to the $\nu i_{13/2}$ band, thus creating a scenario where an adiabatic crossing between these latter bands is plausible. The concept of a low-spin interaction between normal and more-deformed bands was first developed in the $A \approx 175$ region where calculations from a three-band mixing model were employed to help substantiate the existence of this crossing [21]. Therefore, in the present work, we will report on the results of similar calculations performed for bands in ^{131}Nd which also supports the possibility of this type of crossing.

In addition, an analysis of the complete level scheme of ^{131}Nd will be discussed, where a total of seven bands, four of

*Present address: Chemistry Department, Washington University, St. Louis, MO 63130.

†Permanent address: Faculty of Physics, St. Kliment Ohridsky University of Sofia, BG-1164 Sofia, Bulgaria.

‡Present address: NASA Ames Research Laboratory, M/S T27A-1, Moffett Field, CA 94035.

§Present address: Viridien Technologies, Inc., Boxborough, MA 01719.

‖Present address: Department of Physics and Astronomy, State University of New York at Stony Brook, Stony Brook, NY 11794.

¶Present address: Niels Bohr Institute, Copenhagen, DK-2100 Denmark.

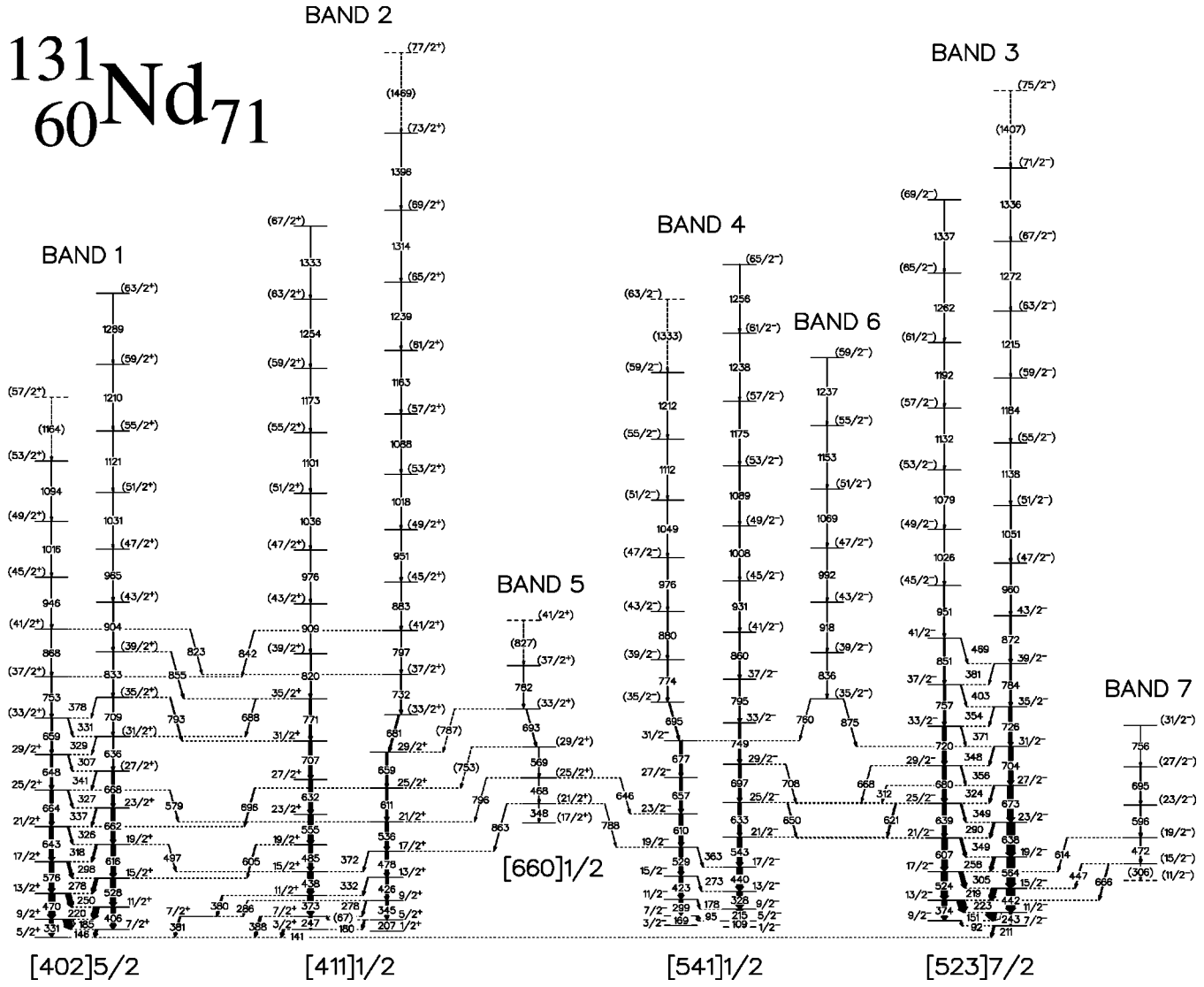

FIG. 1. The level scheme for ^{131}Nd. The widths of the arrows are proportional to the relative intensity of the transition. Tentative transitions are denoted by dashed lines. Spin and parity assignments are explained in the text. The initial configurations for some of the bands are also given.

which are new, were found and extended to high spins ($I \leqslant \frac{77}{2}$). Band properties, such as rotational alignments, $B(M1)/B(E2)$ ratios, and signature splitting, were examined in order to identify the configurations of the observed structures. The signature splitting patterns of the intruder $\nu(h_{9/2}/f_{7/2})[541]1/2$ bands in ^{129,131,133}Nd were inspected and revealed a deformation dependence of this orbital's parentage.

II. EXPERIMENTAL DETAILS

High-spin states in ^{131}Nd were populated in the ^{94}Mo(^{40}Ca,2pn) reaction at a beam energy of 180 MeV. The ^{40}Ca beam was provided by the 88-Inch Cyclotron facility located at the Lawrence Berkeley National Laboratory. The emitted γ rays and charged particles were detected with the Gammasphere spectrometer and the Washington University Microball array, respectively. Approximately 8.3×10^{8} events were recorded when at least one of the 95 CsI detectors from the Microball and at least four of the 92 Compton-suppressed Ge detectors were in prompt coincidence ($\sim$90 ns). The γ rays that were in coincidence with two protons (comprising $\sim$17% of the total events) were sorted into an $E_\gamma\times E_\gamma\times E_\gamma$ cube, which subsequently was analyzed with the RADWARE [22] package. The new level scheme for ^{131}Nd is shown in Fig. 1 and will be discussed in the next section.

The spin assignments proposed for the states in ^{131}Nd were determined through directional correlation of oriented states (DCO) analysis. To facilitate this analysis, an asymmetric matrix was created where the energies of γ rays observed in detectors located at 31.7°, 37.4°, 142.6°, and 148.3° were histogrammed along one axis and coincident γ rays observed in detectors located at 90° were histogrammed along the other axis. DCO ratios were determined by the expression

$$R_{\mathrm{DCO}}=\frac{I_{\gamma_1}(\text{at } \sim 35^\circ \text{ or } \sim 145^\circ, \text{ in coincidence with } \gamma_2 \text{ at } 90^\circ)}{I_{\gamma_1}(\text{at } 90^\circ, \text{ in coincidence with } \gamma_2 \text{ at } \sim 35^\circ \text{ or } \sim 145^\circ)},$$

where I_{γ_1} is the intensity of the γ ray of interest and γ_2 is a stretched $E2(\Delta I=2)$ transition. With the detectors at the given angles, one expects R_{DCO} values of approximately 0.5 for pure dipole transitions ($M1$ and $E1$) and 1.0 for quadrupole transitions ($E2$). The measured DCO ratios are summarized in Table I along with the energy, spin, and parity of the states, as well as the energy and relative intensity of the depopulating γ rays. Weak transitions above states of determined spin, where reliable DCO analysis could not be performed, were assigned multipolarities assuming that the rotational behavior of the particular band persists and the spins are shown in parentheses in Fig. 1. The spins and parities of the states in bands 5, 6, and 7 have been placed within parentheses in Fig. 1 and Table I due to the fact that DCO ratios could not be determined for their linking transitions to states of known spin and parity. For these structures, spin assignments have been based on intensity, energy, and decay considerations. Tentative transitions in Fig. 1 are placed within parentheses and denoted with dashed lines.

III. LEVEL SCHEME

Before the present work, little was known about ^{131}Nd. Decay studies indicate that the ground state likely has a spin of $\frac{5}{2}$, but a parity was not determined [23]. Watson *et al.* [24] observed two strongly coupled structures and one decoupled sequence in ^{131}Nd. In addition to confirming the previously known bands (labeled bands 1, 2, and 3 in Fig. 1), we observed the signature partner to the aforementioned decoupled sequence (band 2) and four new structures. Over 170 new transitions have been placed in the level scheme of ^{131}Nd shown in Fig. 1. One may observe in Fig. 1 that (i) the most intensely populated bands 1, 2 and bands 3, 4 are interlinked, and (ii) for all of the weaker populated bands 5, 6, and 7, decay transitions to the stronger bands are found. Therefore, the relative excitation energies of the seven bands are known. The parity assignments of these structures are largely based on systematics, as outlined in the following paragraphs.

A. Positive-parity structures

Band 1 is a strongly coupled sequence as can be observed in both the level scheme of Fig. 1 and the sample spectra of Fig. 2(a). The band was reported in Ref. [24] up to spin $\frac{23}{2}$, and we have extended it to $\frac{63}{2}$ as seen in Fig. 1. Systematically, two strongly coupled structures are found in $N=71$ nuclei: one with positive parity and no signature splitting in energy and one with negative parity and some signature splitting [25–27]. Figure 3(a) displays the energy of the states for band 1 (minus a rigid rotor energy) plotted versus spin. Essentially no splitting in energy is found between the signatures of band 1 throughout the entire observed portion of the structure. However, signature splitting is observed in the only other strongly coupled sequence (band 3), which is shown in Fig. 3(b). Other band characteristics, e.g., alignment properties and $B(M1)/B(E2)$ ratios (discussed below), lead to a configuration assignment for band 1 with even parity. Based on the systematics and inband properties, positive parity has been assigned to band 1 and a spin of $\frac{5}{2}^+$ is given for the bandhead state. Since this is the lowest level observed in ^{131}Nd from our data, it is possible the $\frac{5}{2}^+$ state in band 1 may be the ground state, which is consistent with the results of the decay study [23] noted above and the $\frac{5}{2}^+$ ground state determined in ^{129}Ce [27]. Several linking transitions between bands 1 and 2 were observed at both low and high spin (Fig. 1), which are a result of the near degeneracies of states as seen in Fig. 3(a) and Table I.

While the $\alpha=-\frac{1}{2}$ signature of band 2 was observed up to spin $\frac{35}{2}$ in Ref. [24], we were able to extend this sequence to $\frac{67}{2}$ as displayed in Fig. 1. The signature partner of band 2 was not reported in Ref. [24]; however, it was observed up to $(\frac{77}{2})$ in the present data. DCO analysis of the strongest inband and linking transitions confirms the spins shown in Fig. 1 for band 2. As a result of the number and nature of the interactions between bands 1 and 2 (where several of the linking transitions were determined to have $E2$ multipolarity; see Table I), they likely have the same parity; therefore, band 2 is also assigned positive parity. At lower spins, large energy splitting is observed in Fig. 3(a) between the signatures of this structure. Although the negative signature is initially favored, an inversion occurs at $\frac{41}{2}$ and the positive signature quickly becomes the yrast sequence of the nucleus above $\frac{49}{2}$. The adiabatic crossing observed between the positive signature of band 2 and band 5 is responsible for this unusual behavior, and has been discussed in an earlier work [19]. Sample spectra for the positive and negative signatures of band 2 are shown in Figs. 2(b) and 2(c), respectively. Transitions from band 5 in coincidence with the positive signature of band 2 are also observed in Fig. 2(b).

The sequence labeled as band 5 in Fig. 1 was observed for the first time in our experiment. Since this structure strongly interacts with the positive signature of band 2 as seen in Fig. 3(a), band 5 most likely has positive parity and positive signature. Although reliable DCO ratios were not obtained for band 5, the tentative spins are consistent with it having $\alpha=+\frac{1}{2}$. The structure decays primarily into band 2, but weak transitions feeding the negative-parity band 4 were also observed.

B. Negative-parity structures

The strongly coupled band 3 in Fig. 1 was reported previously in Ref. [24] up to spin $\frac{37}{2}$. This structure has been extended to $(\frac{75}{2})$ and spectra for the positive and negative signatures are shown in Figs. 4(a) and 4(b), respectively.

TABLE I. Data for levels and gamma rays in ^{131}Nd.

I_i^{π} [a]	E_{level} (keV)	E_γ (keV) [b]	I_γ [c]	DCO	Multipolarity	Band$_f$ [d]
		Band 1: [402]5/2 $\alpha=+\frac{1}{2}$				
$\frac{9}{2}^+$	331.3	331.3	45(3)	1.1(1)	$E2$	1
		185.0	93(5)	0.66(5)	$M1/E2$	1
$\frac{13}{2}^+$	801.7	470.4	71(4)	1.01(6)	$E2$	1
		250.3	52(3)	0.63(5)	$M1/E2$	1
$\frac{17}{2}^+$	1378.0	576.3	57(4)	0.93(6)	$E2$	1
		298.2	26(2)	0.60(6)	$M1/E2$	1
$\frac{21}{2}^+$	2021.4	643.4	48(3)	1.01(7)	$E2$	1
		325.5	12(1)		$M1/E2$	1
$\frac{25}{2}^+$	2685.4	664.0	36(3)	1.04(8)	$E2$	1
		327.0	9.1(9)		$M1/E2$	1
		579.0	6.1(6)		$E2$	2
$\frac{29}{2}^+$	3332.9	647.5	28(2)	0.97(9)	$E2$	1
		307.4	7.8(9)		$M1/E2$	1
$(\frac{33}{2}^+)$	3991.6	658.7	19(2)		$E2$	1
		330.8	5.6(7)		$M1/E2$	1
$(\frac{37}{2}^+)$	4744.7	753.1	15(1)		$E2$	1
$(\frac{41}{2}^+)$	5612.3	867.6	7.4(9)		$E2$	1
		823.3	3.3(4)		$E2$	2
$(\frac{45}{2}^+)$	6558.5	946.2	7.1(9)		$E2$	1
$(\frac{49}{2}^+)$	7574.5	1016.0	4.7(6)		$E2$	1
$(\frac{53}{2}^+)$	8669	1094	<3		$E2$	1
$(\frac{57}{2}^+)$	(9833)	(1164)	<3		$E2$	1
		Band 1: [402]5/2 $\alpha=-\frac{1}{2}$				
$\frac{7}{2}^+$	145.9	145.9	N/D [e]	0.62(3)	$M1/E2$	1
$\frac{11}{2}^+$	551.4	405.5	51(3)	0.88(9)	$E2$	1
		220.3	58(3)	0.56(4)	$M1/E2$	1
$\frac{15}{2}^+$	1079.4	528.0	58(3)	1.12(8)	$E2$	1
		277.9	34(2)	0.66(7)	$M1/E2$	1
$\frac{19}{2}^+$	1695.4	616.0	53(3)	1.04(8)	$E2$	1
		318.0	19(2)	0.56(4)	$M1/E2$	1
		496.9	4.5(5)		$E2$	2
$\frac{23}{2}^+$	2357.6	662.2	43(3)	1.15(9)	$E2$	1
		336.9	12(1)	0.61(7)	$M1/E2$	1
$(\frac{27}{2}^+)$	3025.7	668.1	30(3)		$E2$	1
		340.6	7.6(8)		$M1/E2$	1
$(\frac{31}{2}^+)$	3661.6	635.9	14(2)		$E2$	1
		328.5	4.4(6)		$M1/E2$	1
$(\frac{35}{2}^+)$	4370.6	709.0	8.6(9)		$E2$	1
		378.3	3.2(5)		$M1/E2$	1
		792.7	9.7(8)	1.02(9)	$E2$	2
$(\frac{39}{2}^+)$	5203.5	832.9	10(1)		$E2$	1
		855.1	5.4(5)		$E2$	2
$(\frac{43}{2}^+)$	6107.0	903.5	7.8(9)		$E2$	1
$(\frac{47}{2}^+)$	7071.9	964.9	4.5(6)		$E2$	1
$(\frac{51}{2}^+)$	8103	1031	<3		$E2$	1
$(\frac{55}{2}^+)$	9224	1121	<3		$E2$	1
$(\frac{59}{2}^+)$	10434	1210	<3		$E2$	1
$(\frac{63}{2}^+)$	11723	1289	<3		$E2$	1

TABLE I. (*Continued*).

I_i^{π} [a]	E_{level} (keV)	E_γ (keV) [b]	I_γ [c]	DCO	Multipolarity	Band$_f$ [d]
		Band 2: [411]1/2 $\alpha=+\frac{1}{2}$				
$\frac{5}{2}^+$	320.8	207.1	8.2(9)	1.1(1)	$E2$	2
		179.9	12.2(8)	0.8(1)	$M1/E2$	2
$\frac{9}{2}^+$	665.9	345.1	28(2)	0.91(9)	$E2$	2
		278.2	9.6(9)	0.4(1)	$M1/E2$	2
		285.9	3.4(5)		$M1/E2$	
$\frac{13}{2}^+$	1092.0	426.1	28(2)	1.03(7)	$E2$	2
		331.6	9.1(9)	0.87(9)	$M1/E2$	2
$\frac{17}{2}^+$	1569.9	477.9	37(2)	1.03(7)	$E2$	2
		372.0	5.4(7)		$M1/E2$	2
$\frac{21}{2}^+$	2105.9	536.0	40(2)	1.03(7)	$E2$	2
$\frac{25}{2}^+$	2716.7	610.8	26(2)	1.02(8)	$E2$	2
		695.5	10(1)		$E2$	1
$\frac{29}{2}^+$	3375.8	659.1	20(2)	0.93(9)	$E2$	2
$(\frac{33}{2}^+)$	4057.2	681.4	16(1)		$E2$	2
$(\frac{37}{2}^+)$	4788.8	731.6	13(1)		$E2$	2
$(\frac{41}{2}^+)$	5585.8	797.0	6.6(5)		$E2$	2
		841.7	5.0(6)		$E2$	1
$(\frac{45}{2}^+)$	6468.6	882.8	9.2(9)		$E2$	2
$(\frac{49}{2}^+)$	7419.7	951.1	6.1(6)		$E2$	2
$(\frac{53}{2}^+)$	8437.7	1018.0	4.9(6)		$E2$	2
$(\frac{57}{2}^+)$	9525.7	1088.0	3.5(5)		$E2$	2
$(\frac{61}{2}^+)$	10688.2	1162.5	3.0(5)		$E2$	2
$(\frac{65}{2}^+)$	11927	1239	<3		$E2$	2
$(\frac{69}{2}^+)$	13241	1314	<3		$E2$	2
$(\frac{73}{2}^+)$	14637	1396	<3		$E2$	2
$(\frac{77}{2}^+)$	(16106)	(1469)	<3		$E2$	2
		Band 2: [411]1/2 $\alpha=-\frac{1}{2}$				
$\frac{3}{2}^+$	140.9	140.9	N/D [e]	0.7(1)	$M1/E2$	1
$\frac{7}{2}^+$	387.7	246.8	36(2)	0.98(6)	$E2$	2
		(67)	<3		$M1/E2$	2
		387.7	22(1)	0.58(5)	$M1/E2$	1
$\frac{11}{2}^+$	760.6	372.9	62(3)	0.92(5)	$E2$	2
		379.7	14.0(9)	1.04(9)	$E2$	
$\frac{15}{2}^+$	1198.6	438.0	64(3)	1.02(5)	$E2$	2
$\frac{19}{2}^+$	1683.5	484.9	49(2)	0.94(5)	$E2$	2
		604.5	10(1)	1.0(1)	$E2$	1
$\frac{23}{2}^+$	2238.9	555.4	58(3)	0.93(5)	$E2$	2
$\frac{27}{2}^+$	2870.7	631.8	48(3)	1.03(6)	$E2$	2
$\frac{31}{2}^+$	3578.0	707.3	38(2)	0.98(6)	$E2$	2
$\frac{35}{2}^+$	4348.9	770.9	21(1)	1.1(1)	$E2$	2
		687.8	3.7(4)		$E2$	1
$(\frac{39}{2}^+)$	5168.8	819.9	10.0(9)		$E2$	2
$(\frac{43}{2}^+)$	6077.6	908.8	5.2(7)		$E2$	2
$(\frac{47}{2}^+)$	7053.7	976.1	3.1(5)		$E2$	2
$(\frac{51}{2}^+)$	8090	1036	<3		$E2$	2
$(\frac{55}{2}^+)$	9191	1101	<3		$E2$	2
$(\frac{59}{2}^+)$	10364	1173	<3		$E2$	2

TABLE I. (*Continued*).

I_i^{π} [a]	E_{level} (keV)	E_γ (keV) [b]	I_γ [c]	DCO	Multipolarity	Band$_f$ [d]
$(\frac{63}{2}^+)$	11618	1254	<3		$E2$	2
$(\frac{67}{2}^+)$	12951	1333	<3		$E2$	2
		Band 3: [523]7/2 $\alpha=+\frac{1}{2}$				
$\frac{9}{2}^-$	302.8	92.2	N/D [e]		$M1/E2$	3
$\frac{13}{2}^-$	676.9	374.1	53(3)	0.94(9)	$E2$	3
		223.3	81(4)	0.57(4)	$M1/E2$	3
$\frac{17}{2}^-$	1201.0	524.1	74(4)	0.98(6)	$E2$	3
		305.1	45(3)	0.41(3)	$M1/E2$	3
$\frac{21}{2}^-$	1808.1	607.1	65(3)	1.01(8)	$E2$	3
		349.1	24(2)	0.40(4)	$M1/E2$	3
$\frac{25}{2}^-$	2447.0	638.9	47(3)	0.96(8)	$E2$	3
		348.6	15(2)	0.53(4)	$M1/E2$	3
		621.4	15(1)	1.0(1)	$E2$	4
$\frac{29}{2}^-$	3126.6	679.6	47(3)	1.07(8)	$E2$	3
		355.6	11(1)	0.51(5)	$M1/E2$	3
		667.8	3.7(7)		$E2$	4
$\frac{33}{2}^-$	3846.1	719.5	42(2)	0.90(7)	$E2$	3
		371.3	8.2(9)	0.57(8)	$M1/E2$	3
$\frac{37}{2}^-$	4603.7	757.2	25(2)	0.97(8)	$E2$	3
		403.2	7.7(9)		$M1/E2$	3
$\frac{41}{2}^-$	5454.0	850.7	15.2(9)	0.95(9)	$E2$	3
		468.6	3.8(6)		$M1/E2$	3
$(\frac{45}{2}^-)$	6405.7	951.3	10(1)		$E2$	3
$(\frac{49}{2}^-)$	7431.1	1025.8	6.6(7)		$E2$	3
$(\frac{53}{2}^-)$	8510.4	1079.3	4.1(5)		$E2$	3
$(\frac{57}{2}^-)$	9641.9	1131.5	3.4(5)		$E2$	3
$(\frac{61}{2}^-)$	10834	1192	<3		$E2$	3
$(\frac{65}{2}^-)$	12096	1262	<3		$E2$	3
$(\frac{69}{2}^-)$	13433	1337	<3		$E2$	3
		Band 3: [523]7/2 $\alpha=-\frac{1}{2}$				
$\frac{7}{2}^-$	210.6	210.6	N/D [e]	0.81(9)	$E1$	1
$\frac{11}{2}^-$	453.2	242.6	25(2)	1.05(8)	$E2$	3
		150.5	120(7)	0.51(5)	$M1/E2$	3
$\frac{15}{2}^-$	895.6	442.4	≡100	1.00(4)	$E2$	3
		218.9	56(3)	0.34(4)	$M1/E2$	3
$\frac{19}{2}^-$	1459.5	563.9	95(5)	1.02(5)	$E2$	3
		258.4	28(2)	0.43(4)	$M1/E2$	3
$\frac{23}{2}^-$	2097.4	637.9	89(5)	0.99(6)	$E2$	3
		289.7	20(1)	0.41(4)	$M1/E2$	3
$\frac{27}{2}^-$	2770.5	673.1	67(3)	0.94(6)	$E2$	3
		323.6	13(1)	0.54(8)	$M1/E2$	3
		311.7	5.3(7)		$M1/E2$	4
$\frac{31}{2}^-$	3474.4	703.9	54(3)	1.04(7)	$E2$	3
		347.9	11.8(9)	0.57(8)	$M1/E2$	3
$\frac{35}{2}^-$	4200.3	725.9	36(2)	1.02(7)	$E2$	3
		353.7	7.4(9)		$M1/E2$	3
$\frac{39}{2}^-$	4984.6	784.3	22(1)	0.97(7)	$E2$	3
		380.5	5.2(7)		$M1/E2$	3
$\frac{43}{2}^-$	5856.5	871.9	17(2)	0.94(8)	$E2$	3
$(\frac{47}{2}^-)$	6816.5	960.0	9.7(9)		$E2$	3

TABLE I. (*Continued*).

I_i^{π} [a]	E_{level} (keV)	E_γ (keV) [b]	I_γ [c]	DCO	Multipolarity	Band$_f$ [d]
$(\frac{51}{2}^-)$	7867.0	1050.5	6.6(8)		$E2$	3
$(\frac{55}{2}^-)$	9004.5	1137.5	4.2(7)		$E2$	3
$(\frac{59}{2}^-)$	10188.3	1183.8	3.2(6)		$E2$	3
$(\frac{63}{2}^-)$	11403	1215	<3		$E2$	3
$(\frac{67}{2}^-)$	12675	1272	<3		$E2$	3
$(\frac{71}{2}^-)$	14011	1336	<3		$E2$	3
$(\frac{75}{2}^-)$	(15418)	(1407)	<3		$E2$	3
		Band 4: [541]1/2 $\alpha=+\frac{1}{2}$				
$\frac{5}{2}^-$	299.8	108.6	N/D [e]	1.0(1)	$E2$	4
$\frac{9}{2}^-$	514.8	215.0	63(5)	1.00(8)	$E2$	4
$\frac{13}{2}^-$	842.6	327.8	64(4)	1.00(6)	$E2$	4
$\frac{17}{2}^-$	1282.6	440.0	62(3)	1.03(7)	$E2$	4
$\frac{21}{2}^-$	1825.5	542.9	57(3)	1.03(9)	$E2$	4
$\frac{25}{2}^-$	2458.4	632.9	33(2)	1.05(7)	$E2$	4
		650.3	8.6(9)	1.0(1)	$E2$	3
$\frac{29}{2}^-$	3155.3	696.9	30(2)	0.97(6)	$E2$	4
		708.2	3.9(5)		$E2$	3
$\frac{33}{2}^-$	3904.5	749.2	25(2)	1.00(7)	$E2$	4
$\frac{37}{2}^-$	4699.4	794.9	17(1)	0.92(7)	$E2$	4
$(\frac{41}{2}^-)$	5559.0	859.6	13(1)		$E2$	4
$(\frac{45}{2}^-)$	6490.4	931.4	8.9(8)		$E2$	4
$(\frac{49}{2}^-)$	7498.2	1007.8	5.7(6)		$E2$	4
$(\frac{53}{2}^-)$	8587.6	1089.4	3.7(5)		$E2$	4
$(\frac{57}{2}^-)$	9763	1175	<3		$E2$	4
$(\frac{61}{2}^-)$	11001	1238	<3		$E2$	4
$(\frac{65}{2}^-)$	12257	1256	<3		$E2$	4
$(\frac{69}{2}^-)$	(13516)	(1259)	<3		$E2$	4
		Band 4: [541]1/2 $\alpha=-\frac{1}{2}$				
$\frac{7}{2}^-$	394.1	168.7	20(2)	0.9(1)	$E2$	4
		94.5	11.2(8)		$M1/E2$	4
$\frac{11}{2}^-$	692.6	298.5	35(2)	0.94(6)	$E2$	4
		177.8	7.1(5)	0.55(9)	$M1/E2$	4
$\frac{15}{2}^-$	1115.6	423.0	49(3)	1.02(6)	$E2$	4
		273.4	4.6(5)		$M1/E2$	4
$\frac{19}{2}^-$	1645.0	529.4	46(2)	1.02(4)	$E2$	4
		362.6	3.7(5)		$M1/E2$	4
$\frac{23}{2}^-$	2254.6	609.6	42(2)	1.00(4)	$E2$	4
$\frac{27}{2}^-$	2912.0	657.4	34(2)	1.07(5)	$E2$	4
$\frac{31}{2}^-$	3589.4	677.4	26(2)	1.03(6)	$E2$	4
$\frac{35}{2}^-$	4284.2	694.8	13(1)	0.98(7)	$E2$	4
$(\frac{39}{2}^-)$	5058.4	774.2	11.2(9)		$E2$	4
$(\frac{43}{2}^-)$	5938.2	879.8	7.1(7)		$E2$	4
$(\frac{47}{2}^-)$	6914.4	976.2	4.3(6)		$E2$	4
$(\frac{51}{2}^-)$	7963.8	1049.4	3.4(5)		$E2$	4
$(\frac{55}{2}^-)$	9076	1112	<3		$E2$	4
$(\frac{59}{2}^-)$	10188	1212	<3		$E2$	4
$(\frac{63}{2}^-)$	(11521)	(1333)	<3		$E2$	4

TABLE I. (*Continued*).

I_i^{π} [a]	E_{level} (keV)	E_γ (keV) [b]	I_γ [c]	DCO	Multipolarity	Band$_f$ [d]
			Band 5			
$(\frac{17}{2}^+)$	2085	348	<3		$E2$	5
$(\frac{21}{2}^+)$	2433.2	863.3	4.2(4)		$E2$	2
		788	<3		$E1$	4
$(\frac{25}{2}^+)$	2901.3	468.1	4.2(4)		$E2$	5
		646	<3		$E1$	4
		796	<3		$E2$	2
$(\frac{29}{2}^+)$	3469.8	568.5	6.8(7)		$E2$	5
		(753)	<3		$E2$	2
$(\frac{33}{2}^+)$	4163.0	693.2	6.8(7)		$E2$	5
		(787)	<3		$E2$	2
$(\frac{37}{2}^+)$	4945.4	782.4	4.8(5)		$E2$	5
$(\frac{41}{2}^+)$	(5772)	(827)	<3		$E2$	5
			Band 6			
$(\frac{35}{2}^-)$	4349.0	874.6	4.2(4)		$E2$	3
		759.6	3.0(3)		$E2$	4
$(\frac{39}{2}^-)$	5185.3	836.3	6.0(6)		$E2$	6
$(\frac{43}{2}^-)$	6103.4	918.1	3.6(4)		$E2$	6
$(\frac{47}{2}^-)$	7095	992	<3		$E2$	6
$(\frac{51}{2}^-)$	8164	1069	<3		$E2$	6
$(\frac{55}{2}^-)$	9317	1153	<3		$E2$	6
$(\frac{59}{2}^-)$	10554	1237	<3		$E2$	6
			Band 7			
$(\frac{15}{2}^-)$	1342.4	(306)	<3		$E2$	7
		665.5	10(1)		$M1/E2$	3
		446.7	7.8(8)		$M1/E2$	3
$(\frac{19}{2}^-)$	1814.4	472.0	10(1)		$E2$	7
		613.5	4.4(5)		$M1/E2$	3
$(\frac{23}{2}^-)$	2410.5	596.1	14(1)		$E2$	7
$(\frac{27}{2}^-)$	3105.4	694.9	7.4(8)		$E2$	7
$(\frac{31}{2}^-)$	3861	756	<3		$E2$	7

[a]Spin and parity of the initial state.
[b]Uncertainties in E_γ are 0.2 keV for most transitions except for relatively weak transitions which are 0.5 keV.
[c]Relative intensity of the transition where $I_\gamma(442.4) \equiv 100$.
[d]Band where the final state is located.
[e]Intensity could not be determined.

James *et al.* [28] found that the bandhead is relatively long lived ($\sim$50 ns) and suggested that it feeds the $\frac{7}{2}^+$ state of band 1. However, we were unable to find any coincidence relation between the 145.9- and 210.6-keV transitions from bands 1 and 3, respectively. This, along with the multiple connections between bands 1, 2, 3, 4, and 5, indicates that the bandhead of band 3 decays directly to the possible ground state as shown in Fig. 1. A DCO ratio of 0.81(9) was measured for the linking 210.6-keV transition between bands 1 and 3. While not completely inconsistent with the proposed $E1$ assignment of this γ ray, this DCO ratio is rather large. However, the relatively long lifetime of the bandhead state causes the emitted transition to partially lose its orientation (especially at low spin) which is crucial for obtaining reliable DCO ratios. Thus, the spin and negative-parity assignments of band 3 were based on the systematics of $N=71$ nuclei [25–27,29] and the in-band properties leading to its configuration assignment. Band 3 is the most intensely populated structure for ^{131}Nd below $I=\frac{49}{2}$ (see Table I), which is consistent with it being yrast up to this spin using the given spin assignments. Note that an interaction between bands 3 and 4 near $I=\frac{25}{2}$ was observed (see Fig. 1) where the levels are nearly degenerate.

Both signatures of band 4 are observed for the first time in our data. The $E2$ linking transitions (determined from DCO measurements; see Table I) between bands 3 and 4 confirm

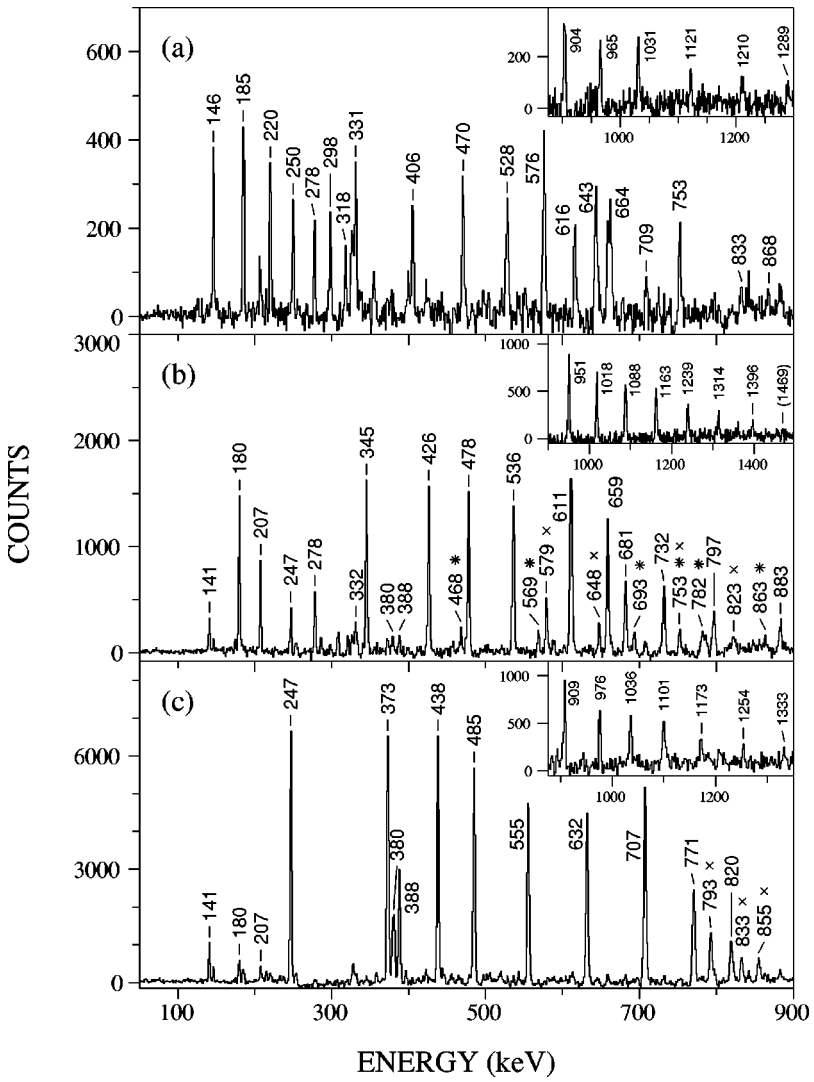

FIG. 2. Sample spectra for (a) band 1, (b) the $\alpha=+\frac{1}{2}$, and (c) $\alpha=-\frac{1}{2}$ signatures of band 2. In panel (a), the main spectrum is a result of summing the double coincidence gates of the 647.5 with the 664.0-keV transitions and the 635.9 with the 668.1-keV transitions. The inset in panel (a) displays the high-energy γ rays observed in the negative signature of band 1. The main spectrum in panel (b) was produced by summing many coincidence spectra. Peaks denoted with $\times$ or * are associated with bands 1 or 5, respectively. The inset, which is also a sum of many coincidence spectra, displays the high-energy γ rays in this signature of band 2. A sum of coincidence spectra produced both the main and insert spectra of panel (c). Peaks marked with $\times$ are related to band 1 and the high-energy transitions are shown in the inset.

the spins assigned to band 4 in Fig. 1 and indicate that these structures likely have the same parity. Since we assigned negative parity for band 3, negative parity is also suggested for band 4. In the sample spectra shown in Figs. 4(c) and 4(d), one can observe the in-band transitions up to the highest spins of $\frac{65}{2}^-$ and ($\frac{63}{2}^-$) for the $\alpha=+\frac{1}{2}$ and $\alpha=-\frac{1}{2}$ signatures, respectively. The transitions from bands 3 and 6 that appear in Figs. 4(c) and 4(d), respectively, can be explained by the corresponding coincidence relations presented in the level scheme of Fig. 1. As shown in Fig. 3(b), there is little signature splitting in band 4 initially, but the positive signature becomes energetically favored as the angular momentum increases. However, at spin $\frac{39}{2}$, an inversion occurs and the negative signature becomes the favored sequence. A discussion of this signature inversion follows in a later section.

A new decoupled sequence that feeds bands 3 and 4 was observed in the data and has been labeled as band 6 in Fig. 1. The tentative spin assignments are based on the intensity (see Table I) of the structure. From inspection of Fig. 3(b), one can see that band 6 may interact with the negative signature of band 4 at $I=\frac{35}{2}$; therefore, we tentatively assign negative parity to band 6. A spectrum of band 6 is shown in Fig. 5(a) where one can observe the in-band transitions, the linking 874.6-keV γ ray, and a few transitions from band 3.

Another weak sequence of γ rays has been observed feeding band 3 and is labeled band 7 in Fig. 1. Negative parity was tentatively assigned to this structure and the spins were assigned in a similar manner as bands 5 and 6. A spectrum of band 7 is given in Fig. 5(b) where many low-spin transitions from band 3 can also be seen.

IV. CONFIGURATION ASSIGNMENTS

Watson *et al.* [24] had suggested that the [402]5/2 and [523]7/2 orbitals were responsible for the strongly coupled

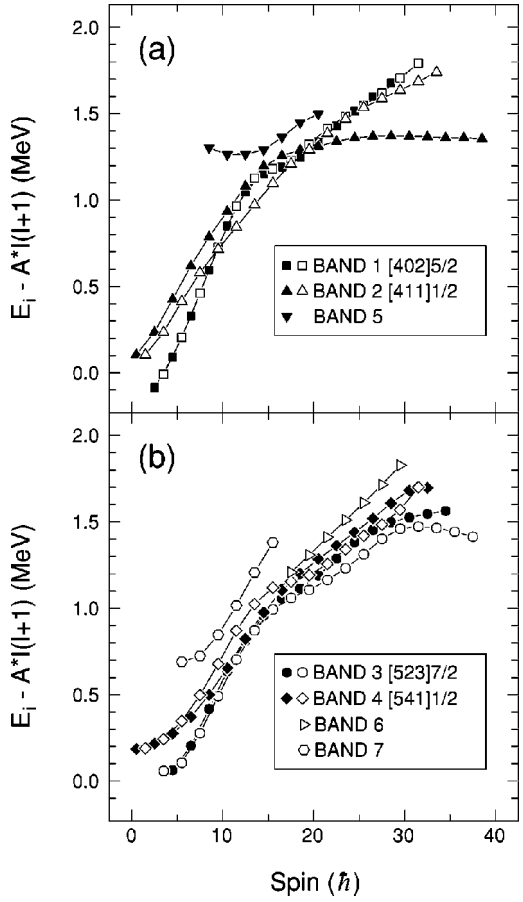

FIG. 3. The energy of the states (minus a rigid rotor) observed in ^{131}Nd versus spin. The positive-parity structures are shown in panel (a), while the negative-parity structures are in panel (b). The moment of inertia parameter was set to $A=0.0097$ MeV. The positive and negative signatures are denoted by solid and open symbols, respectively. Initial configurations for some of the bands are also labeled in the legends.

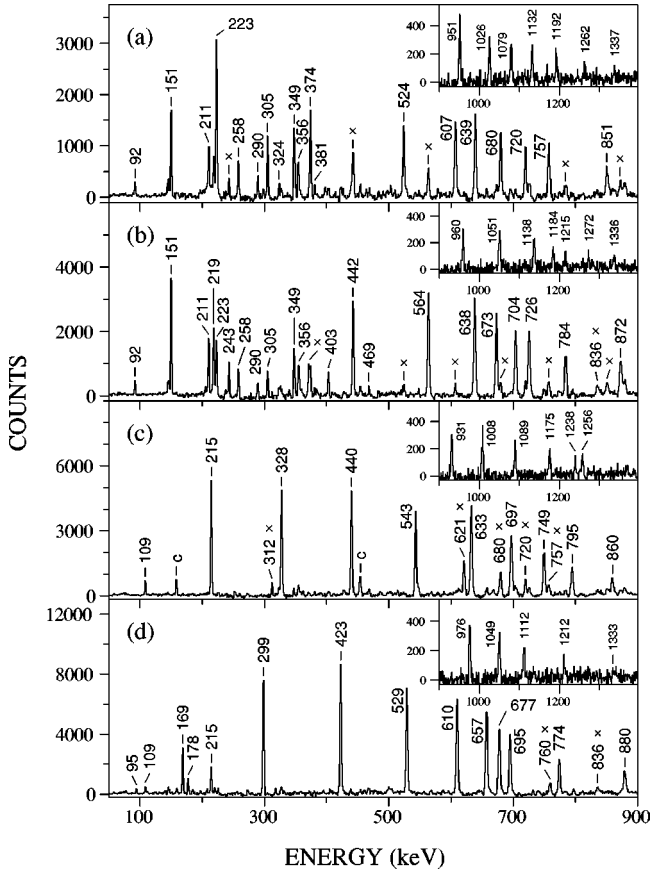

FIG. 4. Spectra for the (a) $\alpha=+\frac{1}{2}$ and (b) $\alpha=-\frac{1}{2}$ signatures of band 3 and the (c) $\alpha=+\frac{1}{2}$ and (d) $\alpha=-\frac{1}{2}$ signatures of band 4. All of the spectra are a result from summing many coincidence spectra of the given band. Peaks denoted only with $\times$ in panels (a) and (b) are transitions from their respective signature partners. In panel (c), peaks marked with ''c'' are contaminate γ rays, while peaks marked with $\times$ are associated with band 3. Transitions from band 6 which are in coincidence with band 4 are marked with $\times$ in panel (d).

structures in ^{131}Nd, but because of limited information on the band structure at that time, they were not able to propose definitive configuration assignments. In order to help identify the active orbitals nearest to the Fermi surface at $N=71$, a neutron single-particle diagram has been provided in Fig. 6. Total Routhian surface (TRS) [7] calculations predict a ground-state deformation near $\beta_2=0.28$ for ^{131}Nd. For a prolate deformation of this size, one can deduce from Fig. 6 that bands based on the $d_{5/2}[402]5/2$, $h_{11/2}[523]7/2$, and $d_{3/2}[411]1/2$ orbitals should be observed at relatively low energies. Although the $(h_{9/2}/f_{7/2})[541]1/2$, $i_{13/2}[660]1/2$, and $(f_{7/2}/h_{9/2})[530]1/2$ orbitals are energetically higher lying, increasing nuclear rotation will bring these low-K structures closer to the Fermi surface. Band characteristics such as alignment behavior, $B(M1)/B(E2)$ ratios, and signature splitting were considered to associate the observed bands in ^{131}Nd with the orbitals noted above.

A. Alignments and band crossings

The rotational alignments of the bands in ^{131}Nd are plotted versus frequency in Fig. 7. Harris parameters [32] of $\mathcal{J}_0=17\,\hbar^2/\mathrm{MeV}$ and $\mathcal{J}_1=26\,\hbar^4/\mathrm{MeV}^3$ were used to subtract the angular momentum of the collective core. The observed crossings are labeled in Fig. 7 using the standard alphabetic labeling scheme [20], which is summarized in Table II in terms of the orbital's parity, signature (π,α), and configuration at zero rotational frequency.

1. Positive-parity structures

In Fig. 7(a), a large gain in alignment ($\Delta i=8.7\hbar$) can be observed at a crossing frequency of $\hbar\omega_c=0.32$ MeV for band 1. The only quasiparticles near the Fermi surface that can align at this low frequency and produce the large alignment gain are the $h_{11/2}$ quasiprotons. The E_pF_p band crossing is well known in the mass 130 region and the alignment gain and crossing frequency are consistent with the first proton crossings observed in other $A\approx130$ nuclei [33]. Band 1 undergoes a second crossing at $\hbar\omega_c\approx0.48$ MeV and gains $\sim3\hbar$ in alignment. The next possible proton crossing is not predicted to occur until very high frequencies ($\hbar\omega>1$ MeV); therefore, this second crossing is likely a result of a

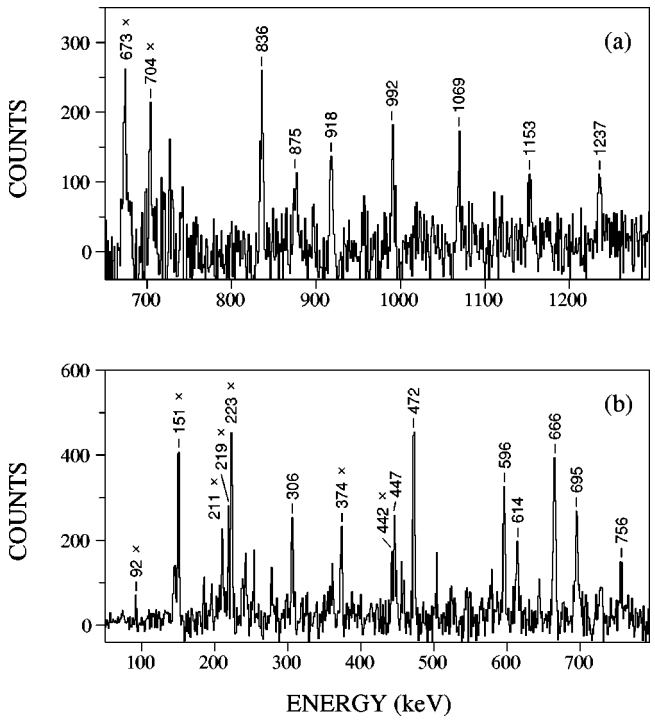

FIG. 5. Spectra for (a) band 6 and (b) band 7. Both panels are a result of summing many coincidence spectra from the given bands. Transitions from band 3 are marked with × in panels (a) and (b).

pair of neutrons aligning. Cranked shell model (CSM) [34] calculations were performed for the quasineutrons and the results are shown in Fig. 8. An alignment of the E and F quasineutrons is predicted to occur near $\hbar\omega = 0.5$ MeV (denoted by ω_{EF} in Fig. 8); thus, the EF alignment is the most probable cause of the second crossing in band 1. The

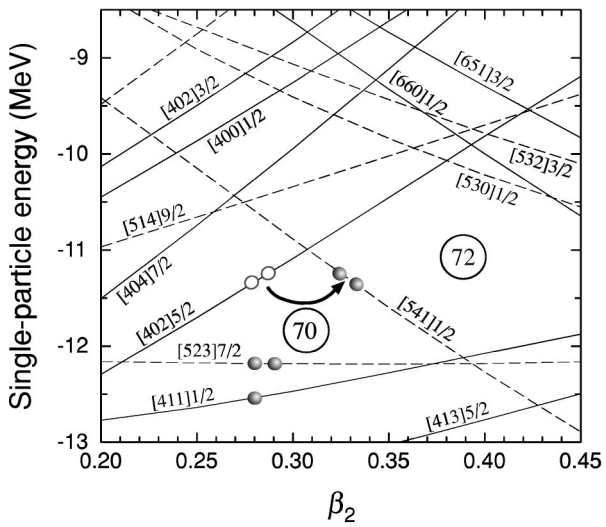

FIG. 6. Neutron single-particle levels as a function of quadrupole deformation (where $\beta_4 = 0$ and $\gamma = 0°$) calculated using the Woods-Saxon potential [30] with parameters given in Ref. [31]. A schematic representation of how the crossing between normal and more-deformed structures occurs is also presented in the figure and discussed in the text.

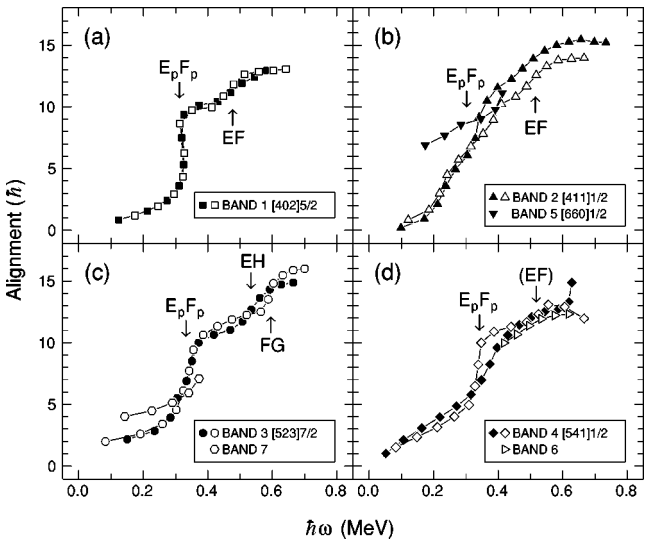

FIG. 7. The rotational alignment plotted versus frequency for (a) band 1, (b) bands 2 and 5, (c) bands 3 and 7, and (d) bands 4 and 6 in ^{131}Nd. Harris parameters of $\mathcal{J}_0 = 17\hbar^2/\text{MeV}$ and $\mathcal{J}_1 = 26\hbar^4/\text{MeV}^3$ were used to subtract the angular momentum of the collective core. The positive and negative signatures are denoted by solid and open symbols, respectively. Initial configurations of some of the bands are also given in the legends.

strongly coupled nature of the band and the lack of signature splitting observed in Fig. 3(a) suggest a configuration with relatively high K. By inspecting Fig. 6, one can see that the [402]5/2, [523]7/2, and [404]7/2 high-K orbitals are closest to the Fermi surface in ^{131}Nd. However, the observed EF crossing in band 1 eliminates the [523]7/2 possibility (due to Pauli blocking arguments) and $B(M1)/B(E2)$ ratios, discussed in a following section, clearly indicate that between the two positive-parity orbitals, band 1 should be associated with the [402]5/2 orbital. This assignment is consistent with similar structures found in the $N = 71$ isotones $^{127}_{56}$Ba [25], $^{129}_{58}$Ce [26], and $^{133}_{62}$Sm [29].

As stated earlier, the multiple interactions between bands 1 and 2 suggest that these structures have the same parity; therefore, band 2 also has positive parity. This structure exhibits a significant amount of signature splitting at lower spin

TABLE II. Alphabetic quasiparticle labeling scheme for ^{131}Nd.

Label	$(\pi,\alpha)_n$ [a]	Configuration [b]	Label	$(\pi,\alpha)_n$ [a]	Configuration [b]
		Quasineutrons			
A	$(+,+\frac{1}{2})_1$	[402]5/2	B	$(+,-\frac{1}{2})_1$	[402]5/2
C	$(+,+\frac{1}{2})_2$	[411]1/2	D	$(+,-\frac{1}{2})_2$	[411]1/2
E	$(-,-\frac{1}{2})_1$	[523]7/2	F	$(-,+\frac{1}{2})_1$	[523]7/2
G	$(-,-\frac{1}{2})_2$	[541]1/2	H	$(-,+\frac{1}{2})_2$	[541]1/2
		Quasiprotons			
E_p	$(-,-\frac{1}{2})_1$	$h_{11/2}$	F_p	$(-,+\frac{1}{2})_1$	$h_{11/2}$

[a]Parity (π) and signature (α) of the orbital. The subscript n numbers the quasiparticles' excitations of a specific signature and parity starting with the lowest in energy at $\hbar\omega = 0$ MeV.
[b]Configuration of the orbital at $\hbar\omega = 0$ MeV.

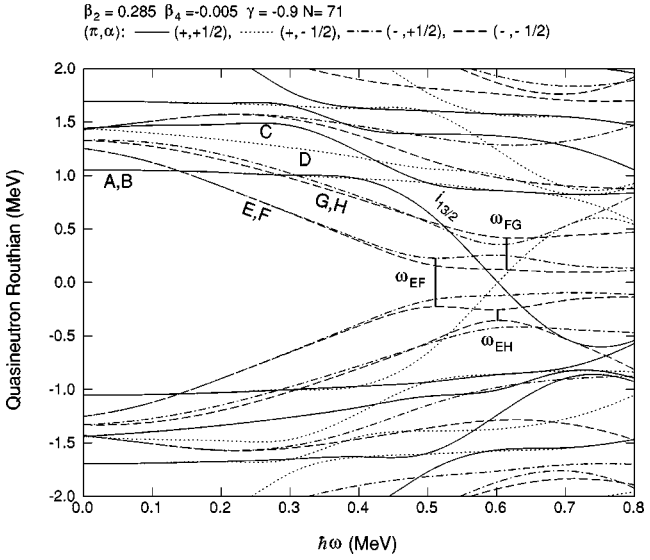

FIG. 8. Cranked shell model calculations for quasineutrons in ^{131}Nd. The deformation parameters (shown at the top of the figure) were determined by TRS calculations. Interpretation of the lines is displayed at the top of the figure. Explanation of the orbital labeling scheme is given in Table II.

[see Fig. 3(a)], indicating that it is likely a low-K sequence. We have assigned the [411]1/2 configuration to the lower spin region of band 2 as this is the nearest low-K, positive-parity orbital to the Fermi surface (see Fig. 6). The alignment of the negative signature of band 2, shown in Fig. 7(b), displays that the sequence undergoes the E_pF_p and EF crossings at $\hbar\omega_c \approx 0.3$ and 0.5 MeV, respectively. The crossing frequencies and alignment gains ($\sim 9.5\hbar$ and $\sim 3\hbar$, respectively) are consistent with the alignments observed in the [402]5/2 band. An additional gain of $\sim 2\hbar$ in alignment occurs in the positive signature, as compared with the negative signature, of band 2 at $\hbar\omega_c \approx 0.34$ MeV. This is due to the adiabatic crossing between bands 2 and 5 noted previously and observed in Fig. 3(a). An exchange of configurations between the highly aligned band 5 and band 2, discussed in Ref. [19] and below, causes the additional alignment. At low frequency (<0.3 MeV), an interaction is observed in both signatures of band 2 that is not seen in the other ^{131}Nd bands. This behavior will be discussed in detail in Sec. V. It should also be noted that the $\frac{7}{2}^+$ state located between bands 1 and 2 in Fig. 1 may possibly be the bandhead of another structure based on the [404]7/2 configuration. Unfortunately, there is no evidence of a band built on this state in the present data.

The large initial alignment ($\sim 7\hbar$) of band 5, shown in Fig. 7(b), leaves few possibilities for its configuration. Since the initial alignment is less than that gained by the E_pF_p crossing ($\sim 9\hbar$) observed in other bands in ^{131}Nd, band 5 is unlikely to be a three quasiparticle structure. According to Fig. 6, the closest orbital that can produce such a large amount of alignment is the [660]1/2; therefore, band 5 has been assigned this configuration. The adiabatic crossing with the $\alpha = +\frac{1}{2}$ signature of band 2 implies an exchange of configurations between the bands; hence it has been proposed that the $\nu i_{13/2}$ sequence continues in band 2 above $I = \frac{33}{2}$ [19]. Highly deformed bands in ^{133,135,137}Nd [14,17,18] are based upon this orbital and, as discussed in Ref. [19], there is evidence to suggest that the $\nu i_{13/2}$ sequence in ^{131}Nd is also highly deformed. Adiabatic crossings involving the $i_{13/2}$ neutron with normal deformed bands have also been reported in several nearby nuclei [4,29,35].

2. Negative-parity structures

Supporting evidence for the negative-parity assignment of band 3 can be found in its alignment behavior in Fig. 7(c). The band undergoes the proton alignment at $\hbar\omega_c \approx 0.32$ MeV and gains $\Delta i \approx 9.0\hbar$, but the two signatures of band 3 seem to experience different crossings at higher rotational frequencies. While both gain $\sim 3.5\hbar$, crossing frequencies of ~ 0.54 and ~ 0.60 MeV are observed in the positive and negative signatures, respectively. These crossings occur at higher frequencies than the EF alignment in band 1, which suggests that the first neutron crossing is blocked. This blocking implies that band 3 is based upon a $\nu h_{11/2}$ orbital, which is most likely to be the [523]7/2 as it is the nearest $\nu h_{11/2}$ orbital to the ^{131}Nd Fermi surface (see Fig. 6). The $B(M1)/B(E2)$ ratios, discussed in the following section, also confirm this assignment. The crossings observed at high frequencies are likely the EH (at $\hbar\omega_c \approx 0.54$ MeV) and FG (at $\hbar\omega_c \approx 0.60$ MeV) alignments, as the CSM calculations predict them to occur near 0.6 MeV in Fig. 8.

Band 4 likely has a low-K configuration as large signature splitting is observed above $I = \frac{13}{2}$ in Fig. 3(b). It has been previously established that bands 3 and 4 likely have the same (negative) parity; therefore, band 4 is assigned the [541]1/2 configuration since this is the nearest negative-parity, low-K orbital to the Fermi surface (see Fig. 6). This neutron configuration has been shown to drive the nuclear shape to intermediate deformations in the neighboring $^{130}_{59}$Pr [10] and ^{133}Nd [11] nuclei. The gradual increase of alignment at low frequency is likely due to the fact that the chosen Harris parameters are less appropriate for band 4 if it indeed has larger deformation than bands 1, 2, 3, and 7. The larger interaction strength of the E_pF_p crossing is also likely the result of the higher deformation of this [541]1/2 band. A sharp contrast can be observed between the signatures of band 4 in the E_pF_p crossing. The signatures appear to have very different interaction strengths in this crossing region; however, no such signature dependent behavior is caused by the proton alignment in the other ^{131}Nd bands. Perhaps another three-quasiparticle band crosses the [541]1/2 negative signature sequence as it undergoes the proton alignment. This scenario will be addressed in more detail in Sec. V. It is difficult to determine where or if either signature of band 4 experiences the EF alignment. A crossing is observed near 0.6 MeV in the positive signature; however, no such alignment behavior is seen in the negative signature. Small alignment gains ($\sim 1-2\hbar$) are found in both signatures near 0.52 MeV; therefore, we have tentatively assigned these as the EF crossing in Fig. 7(d).

By inspecting Fig. 3(b), one may notice that band 6 is observed at the same spin where band 4 experiences its signature inversion. In Fig. 7(d), it should be noted that the

alignment of band 6 lies just below the positive signature of band 4, which is similar to the $\alpha=-\frac{1}{2}$ sequence of band 4 at lower frequencies ($\hbar\omega<0.33$ MeV). With so little information it is difficult to firmly assign a configuration, but if the negative signature of the [541]1/2 band is crossed by another three quasiparticle band, perhaps band 6 is the continuation of the negative signature of the $[541]1/2\otimes E_pF_p$ band.

A structure similar to band 7 in Fig. 1 has been identified in ^{127}Ba [25] and assigned as the favored signature of the [532]5/2 orbital [36]. On the other hand, γ-vibrational bands have been observed in the ^{132,134}Nd [4,35] nuclei at low energies. Therefore, band 7 may be based on the favored signature of the $h_{11/2}$ neutron coupled with a γ phonon. The alignment of this sequence is shown in Fig. 7(c) and one may observe that it has $\sim 2\hbar$ more alignment than band 3 initially. However, since this difference is consistent with both of the possible assignments, it is not possible to distinguish between the [532]5/2 and $[523]7/2\otimes\gamma$ configurations.

B. $B(M1)/B(E2)$ transition strength ratios

Experimental $B(M1)/B(E2)$ ratios were extracted using the observed γ-ray energies and branching ratios $[\lambda=I_\gamma(I\rightarrow I-2)/I_\gamma(I\rightarrow I-1)]$ according to the standard formula

$$\frac{B(M1:I\rightarrow I-1)}{B(E2:I\rightarrow I-2)}=0.693\frac{E_\gamma^5(I\rightarrow I-2)}{E_\gamma^3(I\rightarrow I-1)}\times\frac{1}{\lambda(1+\delta^2)}\left(\frac{\mu_N}{e\,\mathrm{b}}\right)^2,$$

where E_γ is in MeV. To determine the magnitude of the mixing ratios δ for the $\Delta I=1$ transitions, rotational model calculations [37] were performed using the measured branching ratios and assuming pure K. The resulting $B(M1)/B(E2)$ ratios are plotted in Fig. 9 along with theoretical predictions for possible configurations.

Theoretical calculations of $B(M1)/B(E2)$ ratios were performed with the rotational model form of the $B(E2)$ transition strength [37] and an extended formalism [38] of the geometrical model from Dönau [39] and Frauendorf [40] to determine the $B(M1)$ strength. The measured intrinsic quadrupole moment $Q_0=5.16\,e$ b of ^{132}Nd [41] was assumed for the calculations as no lifetime information is available for ^{131}Nd. While the collective gyromagnetic ratio was determined by $g_R=Z/A$, the g_K values were calculated using a Woods-Saxon potential [30] with the following results for the possible configurations shown in Fig. 9: $g_K([402]5/2)=-0.49$, $g_K([404]7/2)=0.36$, $g_K([411]1/2)=1.90$, $g_K([523]7/2)=-0.32$, and $g_K([541]1/2)=-0.54$.

The $B(M1)/B(E2)$ ratios for band 1 are shown in Fig. 9(a) and are located near 0.7 $(\mu_N/e\,\mathrm{b})^2$. A good agreement is observed between the experimental values and the theoretical calculations for the [402]5/2 orbital. In contrast, the predicted [404]7/2 ratios are an order of magnitude below those observed for band 1 due to the difference in sign of the respective g_K factors. Therefore, we can confidently assign band 1 as the [402]5/2 configuration. Bands 2 and 4 have small $B(M1)/B(E2)$ ratios, as shown in Figs. 9(a) and 9(b), which is expected from low-K structures. Good agreement between the calculated and observed ratios is found for our assignments of bands 2 and 4 as the [411]1/2 and [541]1/2

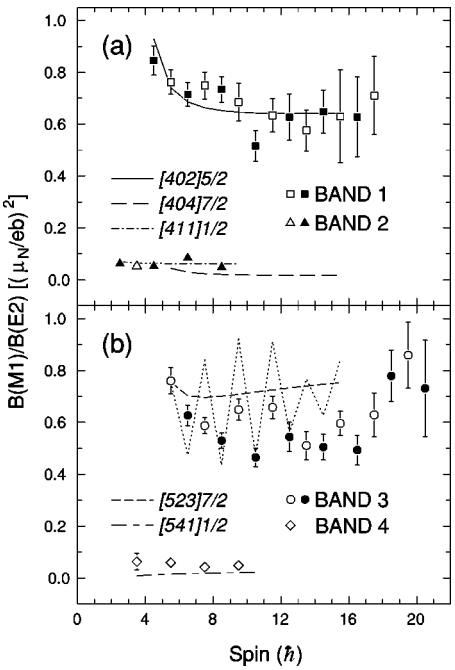

FIG. 9. The experimental (symbols) and theoretical (lines) $B(M1)/B(E2)$ ratios for (a) bands 1 and 2 and (b) bands 3 and 4. The positive and negative signatures are denoted by solid and open symbols, respectively. The dotted line in panel (b) is the result of the [523]7/2 calculation with the signature splitting term $\Delta e'$ as discussed in the text.

structures, respectively. It is worth noting that while the experimental values of band 2 are in agreement with the [404]7/2 calculations, other properties (e.g., spin assignments and signature splitting) do not support this possible configuration for band 2.

Figure 9(b) displays the $B(M1)/B(E2)$ ratios for band 3. Arguments were previously given that this band is based upon an $h_{11/2}$ neutron and a good fit is found with the predicted [523]7/2 values. One may notice the signature splitting in the ratios between $I=\frac{17}{2}$ and $\frac{25}{2}$. The calculated $B(M1)$ strength includes a signature splitting term ($\Delta e'$, where e' is the experimental Routhian), which has been set to zero for all of the previous calculations. In an attempt to reproduce the observed splitting in the $B(M1)/B(E2)$ ratios, we included the $\Delta e'$ term for the [523]7/2 band and the results are shown as the dotted line in Fig. 9(b). One may observe that the calculated splitting is much larger than that experimentally observed. Similar results are found in the $\pi h_{11/2}$ bands of $A\approx 160$ nuclei [42], where it is thought that the high-K orbitals drive the nucleus towards triaxial shapes [43]. The triaxiality would cause larger mixing with lower K states, thus producing the splitting in both the energy and $B(M1)/B(E2)$ ratios. As the mass 130 nuclei are expected to be prone to triaxial driving forces [12,13], a similar scenario is likely producing the signature effects in band 3. Bazzacco *et al.* [14] reproduced both the energy and $B(M1)/B(E2)$ ratio splitting well in the $\nu h_{11/2}$ band of ^{133}Nd using the particle triaxial rotor model with a triaxial deformation parameter of $\gamma=-22°$. Therefore it appears likely that the [523]7/2 band in ^{131}Nd also has some γ de-

TABLE III. Parameters used in the two- and three-band mixing calculations. Values preceded with a ≡ were held constant in the calculations.

Configuration	Band [a]	I_0 ($\times 10^{-2}$ keV^{-1})	C ($\times 10^{6}$ keV^3)	E_0 [b] (keV)	i ($\hbar$)	K ($\hbar$)	$\lvert V\rvert_{gs}$ (keV)	$\lvert V\rvert_{gd}$ (keV)	$\lvert V\rvert_{ds}$ (keV)
			Two-band mixing model						
[402]5/2	*g*	1.500	4.44	26	≡1.0	≡2.5	234		
	s	1.877	27.38	2951	≡10.0	≡2.5			
[523]7/2	*g*	≡1.500	≡4.44	248	≡2.2	≡3.5	254		
	s	1.459	10.31	3131	≡11.0	≡3.5			
[411]1/2	*g*	≡1.500	≡4.44	96	≡1.0	≡0.5	≡244		
fixed $\lvert V\rvert_{gs}$	*s*	0.653	6.06	2251	≡10.0	≡0.5			
[411]1/2	*g*	≡1.500	≡4.44	215	≡1.0	≡0.5	600		
	s	0.653	5.63	2792	≡10.0	≡0.5			
			Three-band mixing model						
[411]1/2	*g*	≡1.500	≡4.44	154	≡1.0	≡0.5	≡244	81	≡244
	d	3.087	9.54	496	≡1.0	≡0.5			
	s	1.902	14.04	3249	≡10.0	≡0.5			

[a] *g*-ground band, *d*-deformed band, *s*-aligned $\pi(h_{11/2})^2$ band.
[b] Unperturbed bandhead energy.

formation below the first band crossing.

V. DISCUSSION

A. Three-band mixing

Low-spin interactions, such as the one observed in band 2, are rarely observed in deformed nuclei. There are cases where rotation stretches the nuclear deformation towards larger values [44], resulting in an alignment gain at lower frequencies; however, this normally occurs when the ground-state deformation is relatively small. As the ground-state deformation for ^{131}Nd is predicted to be somewhat large, $\beta_2 \approx 0.28$, and none of the other bands undergo such an interaction, centrifugal stretching is not likely responsible for the unusual alignment behavior at low frequencies for band 2 [Fig. 7 (b)]. Several bands in the well-deformed nuclei near $A \approx 175$ are also known to have interactions at low spin [21]. Possible explanations have been suggested involving the alignment of various protons or neutrons; however, they are not supported by theoretical calculations and/or the total alignment gained in the bands [21]. An alternative explanation was proposed first for ^{172}Os [45,46] where it was suggested that the ''normal'' band is crossed at low spin by a ''more-deformed'' band. The latter band is created by scattering a pair of *nonaligned* quasiprotons from one orbital into the deformation driving [541]1/2 orbital, which is located near the Fermi suface. A three-band mixing model was developed [that includes parameters describing the normal (g), the more-deformed (d), and the Stockholm aligned (s) bands as well as the interaction strengthes between each] and found to reproduce the data of many bands in the $A \approx 175$ region, suggesting a low frequency crossing by the more-deformed band [21].

The [541]1/2 neutron orbital is close to the Fermi surface in ^{131}Nd as seen in Fig. 1 and Table I. As noted previously, bands involving this neutron in ^{130}Pr [10] and ^{133}Nd [11] were found to have an intermediate deformation. Therefore, the conditions for three-band mixing in ^{131}Nd are comparable with the situation in the $A \approx 175$ nuclei. In our previous work on this nucleus [19], we suggested that the low-frequency interaction in band 2 is a result of a crossing with a more-deformed band. There it has been postulated that a pair of quasineutrons may scatter out of the [402]5/2 orbital and into the [541]1/2 orbital to form the more-deformed band (as schematically demonstrated in Fig. 6). In this light, we have applied the three-band mixing calculation to structures in ^{131}Nd, which is the first attempt to justify such a scenario outside the heavy rare-earth region.

The variables used to describe the unperturbed bands are as follows: the variable moment of inertia (VMI) [47] parameters I_0 (ground-state moment of inertia) and C (restoring force constant), bandhead energy E_0, alignment i, K, and the interaction strengths between the three bands. A two-band calculation was performed first on the negative signature of the [402]5/2 band. As shown in Table III, the only fixed parameters were the alignment and K values of the g and s bands. From Fig. 10(a), one can observe that a good fit was obtained to the experimental data with reasonable parameters. To reduce the number of variables in further calculations, we fixed the I_0 and C values for the g bands to those calculated for the [402]5/2 band. Although the moments of inertia of different bands may flucuate for different configurations, the values should not differ greatly. The negative signature of the [523]7/2 band was calculated holding the aforementioned parameters constant, and the results are shown in Table III and Fig. 10(b). Once again, a good fit was obtained with parameters similar to those of the [402]5/2 band; therefore, our assumption of fixing the g-band parameters seems reasonable.

Two calculations were performed for the negative signature of the [411]1/2 band (note that calculations were not done for the positive signature as the crossing with the $\nu i_{13/2}$

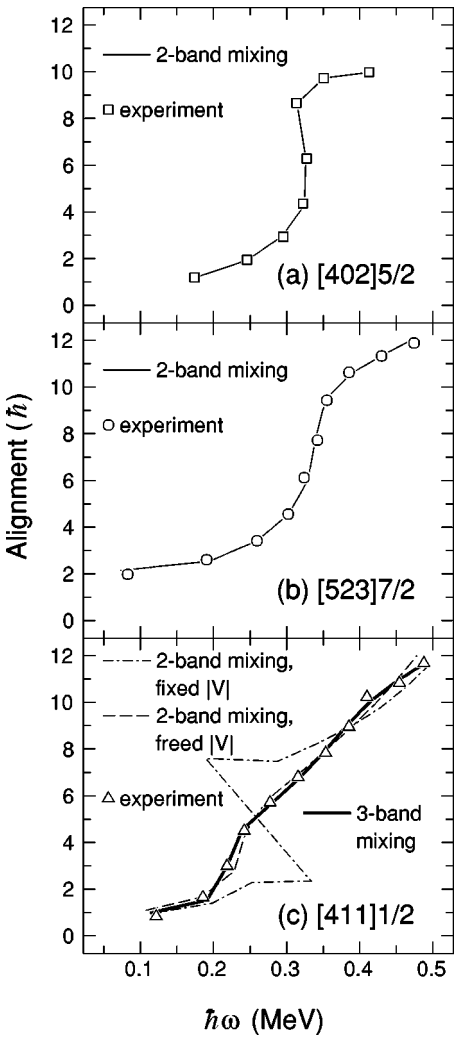

FIG. 10. Experimental (symbols) and calculated (lines) alignment values for the negative signatures of the (a) [402]5/2, (b) [523]7/2, and (c) [411]1/2 bands. Parameters used for the calculated alignments are summarized in Table III and described in the text.

sequence makes for a more complicated situation) using the two-band mixing model. First, the interaction strength between the *g* and *s* bands was fixed to the average of the previously fitted bands. The result is an extremely poor fit as shown in Fig. 10(c). When the interaction strength was allowed to vary, a better fit was produced [Fig. 10(c)], but with inconsistent parameters compared with the previous two bands. In Table III, one can observe that a low moment of inertia value for the *s* band and large interaction strength were required to produce the fit. It would be difficult to explain why the proton crossing in the [411]1/2 band has an interaction strength nearly 2.5 times greater than the previously calculated bands. However, if three-band mixing is considered, a good fit to the data is found [Fig. 10(c)] even with the interaction strengths between the *g* and *s* bands, $|V|_{gs}$ and the *d* and *s* bands, $|V|_{ds}$, fixed to 244 keV. The moment of inertia parameter for the *d* band is similar to the value used for the more-deformed band in the $A \approx 175$ region [21] and it indicates a structure of larger deformation than the normal band. Therefore, the unusual low-spin interaction in the [411]1/2 band appears to be described best with a mixing of the normal, more-deformed, and aligned bands.

A reasonable explanation for the adiabatic crossing between the [411]1/2 and [660]1/2 bands is now available. With a pair of quasineutrons occupying the [541]1/2 orbital in the more-deformed [411]1/2 structures, its deformation may be relatively close to that of the highly deformed [660]1/2 sequence. The decay of the $\nu i_{13/2}$ band into the [541]1/2 band (Fig. 1) indicates that there is a strong likelihood that these negative-parity quasineutrons are involved in the underlying structure of the highly deformed sequence. The occupation of the $h_{9/2}/f_{7/2}$ orbital has been found to play a significant role for highly deformed bands in Pr nuclei [2] and are likely involved in the $\nu i_{13/2}$ bands of Nd nuclei. Since the [660]1/2 and the more-deformed [411]1/2 bands likely have a relatively small deformation difference and similar underlying structures, a scenario for an adiabatic crossing between the two bands is created.

Experimental observation shows no low-spin crossing for the [523]7/2 band; however, from inspecting Fig. 6 one might expect an interaction to occur. The pair of quasineutrons occupying the [402]5/2 orbital could still scatter into the [541]1/2 orbital and yet no such behavior is seen in the $\nu h_{11/2}$ band. A possible explanation for this may be found in a statement made previously in describing band 3. That is, the [523]7/2 band shows characteristics of a structure with γ deformation at lower spins. Nilsson-Strutinsky-BCS calculations indicate that any triaxial deformation (positive or negative) moves the [541]1/2 orbital up in energy; therefore, moving it away from the Fermi surface in ^{131}Nd. If the calculations are correct, then the more-deformed band would be higher in energy and thus not as likely to interact strongly with the *g* and *s* bands.

Known structures in neighboring nuclei were examined to see if similar low-frequency interactions could be observed. In the $N=71$ isotone ^{133}Sm [29], no crossing is observed in the [411]1/2 band; however, it was speculated from TRS calculations that a pair of neutrons initially occupy the [541]1/2 orbital in the core of this structure. An interaction near $\sim$0.3 MeV in the [523]7/2 band has been associated with a crossing of a more-deformed band. This $\nu h_{11/2}$ structure exhibits virtually no signature splitting in energy or $B(M1)/B(E2)$ ratios; therefore it likely has little triaxial deformation and thus the crossing may be seen in the [523]7/2 band of ^{133}Sm but not in ^{131}Nd. A low-spin interaction is not seen in the bands of ^{129}Ce [26], but only structures built upon the [402]5/2, [523]7/2, and the [660]1/2 or [541]1/2 orbitals were reported. Since none of these bands experienced three-band mixing in ^{131}Nd, one would not expect a crossing for the bands in ^{129}Ce. Perhaps the best evidence of this interaction in another nucleus is the ground-state band of ^{132}Nd [35]. Figure 11 plots the alignments of the ground-state bands for ^{130}Nd [48], ^{132}Nd, and ^{134}Nd [4]. Although the $h_{11/2}$ proton crossing is located near $\hbar\omega = 0.35$ MeV for ^{130}Nd and ^{134}Nd, the alignment apparently occurs earlier ($\sim$0.3 MeV) in ^{132}Nd. Such large shifts in the proton crossing frequency are not observed in the even-even Ce nuclei [33], so it is possible that the more-deformed band is interacting with the ground and aligned bands just before

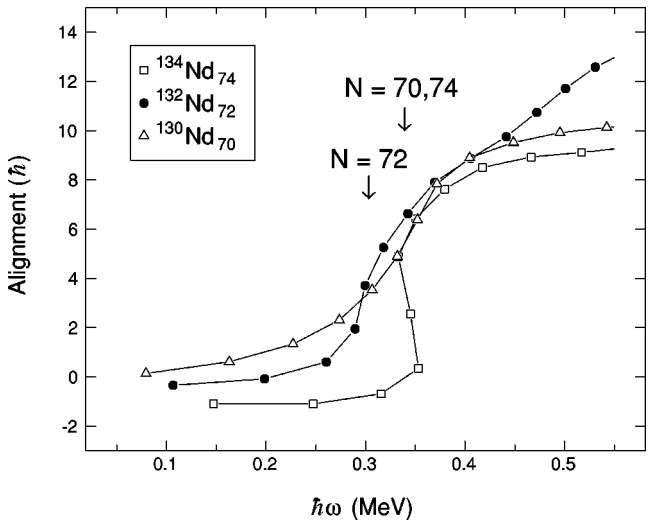

FIG. 11. Alignment plots for the ground-state bands in ^{130,132,134}Nd. Harris parameters of $\mathcal{J}_0 = 17\hbar^2/\mathrm{MeV}$ and $\mathcal{J}_1 = 26\hbar^4/\mathrm{MeV}^3$ were used to subtract the angular momentum of the collective core.

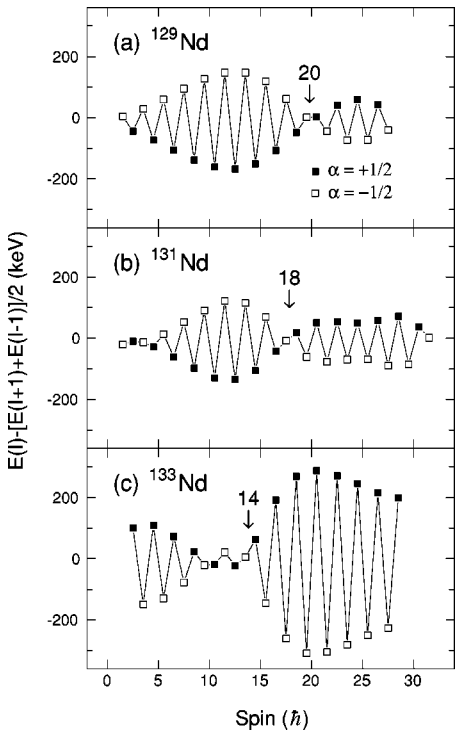

FIG. 12. Signature splitting of the [541]1/2 bands in (a) ^{129}Nd, (b) ^{131}Nd, and (c) ^{133}Nd. The inversion point is marked in each panel with an arrow. The positive and negative signatures are denoted by solid and open symbols, respectively.

and into the proton crossing region. With the two interactions located so close to each other, it may appear as one crossing, but with a lower crossing frequency compared with the neighboring ^{130,134}Nd nuclei as seen in Fig. 11. Three-band mixing calculations were performed for the ground-state band of ^{132}Nd; however, definitive results could not be extracted due to the crossing observed immediately after the proton alignment (possibly caused by an $\nu h_{11/2}$ alignment) as seen in Fig. 11.

B. Signature splitting in the [541]1/2 band

Large energy splitting is expected between the signatures for the [541]1/2 band as the decoupling parameter [37] in $K = 1/2$ bands separates the signatures in energy. Indeed, only the favored positive signature of the proton [541]1/2 band is observed in the $Z = 71$ ^{165,167,169}Lu [49–51] nuclei. However, from Figs. 1 and 3(b), one can see that both signatures of this band are observed, and that the energy splitting at low spin is rather small. Figure 12 plots the energy of a given spin state (I) minus the average of the energies from the states $I+1$ and $I-1$ versus spin for the [541]1/2 bands in ^{129,131,133}Nd in order to amplify signature effects. A few trends can be recognized after inspecting this figure. First, at lower spins the positive signature is found to be most favored initially in ^{129}Nd [52], little splitting is observed in ^{131}Nd, and the negative signature is favored in ^{133}Nd [14]. Since the parentage of the [541]1/2 orbital is mixed between the $h_{9/2}$ and $f_{7/2}$ shells, the favored signature at low spin can help determine which shell contributes the largest component to the wave function. The favored signature α_f can be determined by the j of the shell, where $\alpha_f = \frac{1}{2}(-1)^{j-1/2}$. Therefore, when the the $h_{9/2}$ component is most dominant, $\alpha_f = +\frac{1}{2}$ as in the case for ^{129}Nd [Fig. 12(a)]. In ^{133}Nd [Fig. 12(c)], where $\alpha_f = -\frac{1}{2}$ initially, it appears that the $f_{7/2}$ shell is dominant and in ^{131}Nd [Fig. 12(b)] there is an equal mixture. This trend is likely a result of the increasing deformation as the Nd nuclei become more neutron deficient. The orbital originates from the $f_{7/2}$ shell; therefore at lower deformations (e.g., in ^{133}Nd) one expects this shell to be favored over the $h_{9/2}$. However, at larger deformations the $K = 1/2$ orbital from the $h_{9/2}$ shell crosses the [541]1/2 orbital such that the dominant component is changed. Figure 12 thus displays a nice experimental verification of the ''parentage evolution'' for the [541]1/2 orbital with deformation.

As the angular momentum is increased, the positive signature becomes more energetically favored and in fact an inversion takes place near $I = \frac{21}{2}$ in ^{133}Nd [see Fig. 12(c)]. At higher spins, though, the negative signature becomes favored for all three Nd nuclei. Figure 12 labels where these inversions approximately occur for each of the nuclei, and it can be observed that with increasing N, the inversion happens at a lower spin. The amplitude of the splitting after the inversion also increases with N. As stated previously, since none of the other bands in ^{131}Nd (or ^{129,133}Nd) show similar signature effects after the proton crossing, perhaps there is another three-quasiparticle band which strongly interacts with the negative signature of the [541]1/2 band. There are only a few negative-parity orbitals to consider which may interact with the [541]1/2 band. The best possibility for the interacting structure is the favored signature of the [530]1/2 band after the $\pi h_{11/2}$ alignment. Since the Fermi surface for ^{133}Nd is closest to the [530]1/2 orbital (see Fig. 6), one might expect the crossing to occur at the lowest spin and have the largest effect in this nucleus as compared with ^{129,131}Nd. This may also imply that the two negative-parity $K = 1/2$ orbitals are closer to each other than the calculations in Fig.

6 suggest. However, without knowledge of the bandhead energies of both structures it is difficult to verify this statement.

VI. SUMMARY

Over 170 new transitions have been placed in the level scheme of ^{131}Nd. There is evidence to suggest that the [660]1/2 and [541]1/2 sequences have high and intermediate quadrupole deformations, respectively, while the [523]7/2 band may be triaxially deformed below the proton crossing. Several quasiparticle alignments were observed in the bands, which were interpreted with the cranked shell model. Three-band mixing calculations were performed in order to understand the low-spin crossing in the [411]1/2 band. This crossing was reproduced best by considering a third ''more-deformed'' band interacting with the ground and aligned bands. These results are similar to those found in the $A \approx 175$ region where low-spin interactions are also seen [21]. Inspection of the signature splitting plots for the [541]1/2 bands in ^{129,131,133}Nd reveals a consistent picture of the mixing between $h_{9/2}$ and $f_{7/2}$ parentage for the orbital as deformation increases. Signature inversions at higher spins were also observed in the [541]1/2 bands and are possibly the result of a crossing with another three quasiparticle band.

ACKNOWLEDGMENTS

We would like to give special thanks to D. C. Radford for his software support and to R. A. Bark for use and discussions of the three-band mixing model. Discussions with F. G. Kondev are also gratefully acknowledged. The authors also wish to thank the LBNL operations staff at Gammasphere. This work was funded by the U.S. Department of Energy through Contract Nos. DE-FG02-96ER40983 (University of Tennessee), W-31-109-ENG-38 (Argonne National Laboratory), and DE-FG05-88ER40406 (Washington University). ORNL is managed by Lockheed Martin Energy Research Corporation for the U.S. DOE under Contract No. DE-AC05-96OR22464.

[1] R.M. Clark, I.Y. Lee, P. Fallon, D.T. Joss, S.J. Asztalos, J.A. Becker, L. Bernstein, B. Cederwall, M.A. Deleplanque, R.M. Diamond, L.P. Farris, K. Hauschild, W.H. Kelly, A.O. Macchiavelli, P.J. Nolan, N. O'Brien, A.T. Semple, F.S. Stephens, and R. Wadsworth, Phys. Rev. Lett. **76**, 3510 (1996).

[2] B.H. Smith, L.L. Riedinger, H.Q. Jin, W. Reviol, W. Satula, A. Galindo-Uribarri, D.G. Sarantites, J.N. Wilson, D. LaFosse, and S.M. Mullins, Phys. Lett. B **443**, 89 (1998).

[3] F.G. Kondev, M.A. Riley, D.J. Hartley, T.B. Brown, R.W. Laird, M. Lively, R.K. Sheline, E.S. Paul, D.T. Joss, P.J. Nolan, S.L. Shepherd, R.M. Clark, P. Fallon, D.G. Sarantites, M. Devlin, D.R. LaFosse, F. Lerma, R. Wadsworth, I.M. Hibbert, N.J. O'Brien, and J. Simpson, Phys. Rev. C **60**, 011303(R) (1999).

[4] C.M. Petrache, D. Bazzacco, S. Lunardi, C. Rossi Alvarez, R. Venturelli, R. Burch, P. Pavan, G. Maron, D.R. Napoli, L.H. Zhu, and R. Wyss, Phys. Lett. B **387**, 31 (1996).

[5] A. Galindo-Uribarri, D. Ward, H.R. Andrews, G.C. Ball, D.C. Radford, V.P. Janzen, S.M. Mullins, J.C. Waddington, A.V. Afanasjev, and I. Ragnarsson, Phys. Rev. C **54**, 1057 (1996).

[6] N.J. O'Brien, R. Wadsworth, D.E. Archer, P. Fallon, I.M. Hibbert, D.T. Joss, D.R. LaFosse, P.J. Nolan, E.S. Paul, J. Pfohl, M.A. Riley, D.G. Sarantites, and R. Wyss, Phys. Rev. C **58**, 3212 (1998).

[7] R. Wyss, J. Nyberg, A. Johnson, R. Bengtsson, and W. Nazarewicz, Phys. Lett. B **215**, 211 (1988).

[8] A.V. Afanasjev and I. Ragnarsson, Nucl. Phys. **A608**, 176 (1996).

[9] M.N. Rao, R.V. Ribas, N.H. Medina, J.R.B. Oliveira, M.A. Rizzutto, W.A. Seale, C.M. Petrache, D. Bazzacco, S. Lunardi, C. Rossi Alvarez, T. Scanferla, C.A. Ur, R. Venturelli, F.R. Espinoza-Quiñones, Zs. Podolyák, D. De Acuña, G. de Angelis, M. De Poli, E. Farnea, A. Gadea, D.R. Napoli, L.H. Zhu, A. Dewald, J. Gableske, and P. von Brentano, Phys. Rev. C **58**, R1367 (1998).

[10] F.G. Kondev, M.A. Riley, D.J. Hartley, T.B. Brown, R.W. Laird, M. Lively, R.K. Sheline, R.M. Clark, P. Fallon, D.G. Sarantites, M. Devlin, D.R. LaFosse, F. Lerma, R. Wadsworth, I.M. Hibbert, N.J. O'Brien, E.S. Paul, D.T. Joss, P.J. Nolan, S.L. Shepherd, D.E. Archer, and J. Simpson, Phys. Rev. C **59**, 3076 (1999).

[11] F. Brandolini, N.H. Medina, D. Bazzacco, D. Bucurescu, M. Ionescu-Bujor, R.V. Ribas, C. Rossi Alvarez, C.A. Ur, M. De Poli, G. de Angelis, G. Falconi, S. Lunardi, P. Pavan, R. Burch, and D. De Acuna, Phys. Rev. C **60**, 024310 (1999).

[12] S. Frauendorf and F.R. May, Phys. Lett. **125B**, 245 (1983).

[13] R. Wyss, A. Granderath, R. Bengtsson, P. von Brentano, A. Dewald, A. Gelberg, A. Gizon, J. Gizon, S. Harissopulos, A. Johnson, W. Lieberz, W. Nazarewicz, J. Nyberg, and K. Schiffer, Nucl. Phys. **A505**, 337 (1989).

[14] D. Bazzacco, F. Brandolini, G. Falconi, S. Lunardi, N.H. Medina, P. Pavan, C. Rossi-Alvarez, G. de Angelis, D. De Acuna, M. De Poli, D.R. Naploi, J. Rico, D. Bucurescu, M. Ionescu-Bujor, and C.A. Ur, Phys. Rev. C **58**, 2002 (1998).

[15] R. Janssens and F. Stephens, Nucl. Phys. News **6**, 9 (1996).

[16] D.G. Sarantites, P.-F. Hua, M. Devlin, L.G. Sobotka, J. Elson, J.T. Hood, D.R. LaFosse, J.E. Sarantites, and M.R. Maier, Nucl. Instrum. Methods Phys. Res. A **381**, 418 (1996).

[17] E.M. Beck, F.S. Stephens, J.C. Bacelar, M.A. Deleplanque, R.M. Diamond, J.E. Draper, C. Duyar, and R.J. McDonald, Phys. Rev. Lett. **58**, 2182 (1987).

[18] S. Lunardi, R. Venturelli, D. Bazzacco, C.M. Petrache, C. Rossi-Alvarez, G. de Angelis, G. Vedovato, D. Bucurescu, and C. Ur, Phys. Rev. C **52**, R6 (1995).

[19] D.J. Hartley, W. Reviol, L.L. Riedinger, F.G. Kondev, A. Galindo-Uribarri, D.G. Sarantites, H.Q. Jin, D.R. LaFosse, S.M. Mullins, B.H. Smith, and J.N. Wilson, Phys. Rev. C **60**, 041301(R) (1999).

[20] R. Bengtsson, S. Frauendorf, and F.-R. May, At. Data Nucl. Data Tables **35**, 15 (1986).

[21] R.A. Bark, J. Phys. G **17**, 1209 (1991).
[22] D.C. Radford, Nucl. Instrum. Methods Phys. Res. A **361**, 297 (1995).
[23] P.A. Wilmarth, J.M. Nitschke, R.B. Firestone, and J. Gilat, Z. Phys. A **325**, 485 (1986).
[24] D.C.B. Watson, A.N. James, M.A. Skelton, and J. Simpson, Liverpool University, Annual Report, 1987–1988, p. 29.
[25] A. Dewald, A. Schmidt, G. Alexius, O. Vogel, R.S. Chakrawarthy, D. Bazzacco, P. von Brentano, A. Gizon, J. Gizon, S. Lunardi, D.R. Napoli, P. Pavan, C. Rossi Alvarez, and I. Wiedenhöver, Eur. Phys. J. A **3**, 103 (1998).
[26] A. Galindo-Uribarri, S.M. Mullins, D. Ward, M. Cromaz, J. DeGraaf, T.E. Drake, S. Flibotte, V.P. Janzen, D.C. Radford, and I. Ragnarsson, Phys. Rev. C **54**, R454 (1996).
[27] A. Gizon, J. Genevey, D. Bucurescu, Gh. Căta-Danil, J. Gizon, J. Inchaouh, D. Barnéoud, T. von Egidy, C.F. Liang, B.M. Nyakó, P. Paris, I. Penev, A. Plochocki, E. Ruchowska, C.A. Ur, B. Weiss, and L. Zolnai, Nucl. Phys. **A605**, 301 (1996).
[28] A.N. James, Y. He, I. Jenkins, and M.A. Skelton, Daresbury Laboratory, 1989–1990 Annual Report, Appendix, p. 25.
[29] C.M. Parry, I.M. Hibbert, R. Wadsworth, A.N. Wilson, A.J. Boston, D.T. Joss, P.J. Nolan, E.S. Paul, A. Galindo-Uribarri, V.P. Janzen, D. Ward, S.M. Mullins, P.H. Regan, and R. Wyss, Phys. Rev. C **60**, 054314 (1999).
[30] S. Ćwiok, J. Dudek, W. Nazarewicz, J. Skalski, and T. Werner, Comput. Phys. Commun. **46**, 379 (1987); J. Dudek, A. Majhofer, J. Skalski, T. Werner, S. Ćwiok, and W. Nazarewicz, J. Phys. G **5**, 1359 (1979).
[31] W. Nazarewicz, M.A. Riley, and J.D. Garrett, Nucl. Phys. **A512**, 61 (1990).
[32] S.M. Harris, Phys. Rev. **138**, B509 (1965).
[33] D.J. Hartley, L.L. Riedinger, H.Q. Jin, W. Reviol, B.H. Smith, A. Galindo-Uribarri, D.G. Sarantites, D.R. LaFosse, J.N. Wilson, and S.M. Mullins, Phys. Rev. C **60**, 014308 (1999).
[34] R. Bengtsson and S. Frauendorf, Nucl. Phys. **A327**, 139 (1979); **A314**, 27 (1979).
[35] C.M. Petrache, D. Bazzacco, P. Bednarczyk, G. de Angelis, M. De Poli, C. Fahlander, G. Falconi, E. Farnea, A. Gadea, M. Lunardon, S. Lunardi, N. Marginean, R. Menegazzo, P. Pavan, Zs. Podolyák, C. Rossi Alvarez, C.A. Ur, R. Venturelli, L.H. Zhu, and R. Wyss, Phys. Lett. B **415**, 223 (1997).
[36] D. Ward, H.R. Andrews, V.P. Janzen, D.C. Radford, J.K. Johansson, D. Prévost, J.C. Waddington, A. Galindo-Uribarri, and T.E. Drake, Nucl. Phys. **A539**, 547 (1992).
[37] A. Bohr and B.R. Mottelson, *Nuclear Structure* (Benjamin, New York, 1975), Vol. 2.
[38] V.P. Janzen, Z.-M. Liu, M.P. Carpenter, L.H. Courtney, H.-Q. Jin, A.J. Larabee, L.L. Riedinger, J.K. Johansson, D.G. Popescu, J.C. Waddington, S. Monaro, S. Pilotte, and F. Dönau, Phys. Rev. C **45**, 613 (1992).
[39] F. Dönau, Nucl. Phys. **A471**, 469 (1987).
[40] S. Frauendorf, Phys. Lett. **100B**, 219 (1981).
[41] R. Krücken, A. Dewald, G. Böhm, P. Sala, J. Altmann, K.O. Zell, P. von Brentano, S.A. Forbes, S.M. Mullins, D.J. Thornley, A.J. Kirwan, P.J. Nolan, P.H. Regan, and R. Wadsworth, Nucl. Phys. **A589**, 475 (1995).
[42] D.J. Hartley, T.B. Brown, F.G. Kondev, J. Pfohl, M.A. Riley, S.M. Fischer, R.V.F. Janssens, D.T. Nisius, P. Fallon, W.C. Ma, and J. Simpson, Phys. Rev. C **58**, 2720 (1998).
[43] Y.S. Chen, S. Frauendorf, and L.L. Riedinger, Phys. Lett. B **171**, 7 (1986).
[44] G.D. Symons and A.C. Douglas, Phys. Lett. **24B**, 11 (1967).
[45] J.L. Durell, G.D. Dracoulis, C. Fahlander, and A.P. Byrne, Phys. Lett. **115B**, 367 (1982).
[46] G.D. Dracoulis, R.A. Bark, A.E. Stuchbery, A.P. Byrne, A.M. Baxter, and F. Riess, Nucl. Phys. **A486**, 414 (1988).
[47] M.A.J. Mariscotti, G. Scharff-Goldhaber, and B. Buck, Phys. Rev. **176**, 1864 (1968).
[48] R. Wadsworth, P. Regan, S.M. Mullins, G.J. Gyapong, D.L. Watson, P.J. Nolan, M.J. Godfrey, I. Jenkins, Y.J. He, B.J. Varley, J. Simpson, and W. Gelletly, Z. Phys. A **333**, 411 (1989).
[49] S. Jónsson, J. Lyttkens, L. Carlén, N. Roy, H. Ryde, W. Waluś, J. Kownacki, G.B. Hagemann, B. Herskind, J.D. Garrett, and P.O. Tjøm, Nucl. Phys. **A422**, 397 (1984).
[50] C.-H. Yu, G.B. Hagemann, J.M. Espino, K. Furuno, J.D. Garrett, R. Chapman, D. Clarke, F. Khazaie, J.C. Lisle, J.N. Mo, M. Bergström, L. Carlén, P. Ekström, J. Lyttkens, and H. Ryde, Nucl. Phys. **A511**, 157 (1990).
[51] S. Ogaza, J. Kownacki, M.P. Carpenter, J. Gascon, G.B. Hagemann, Y. Iwata, H.J. Jensen, T. Komatsubara, J. Nyberg, G. Sletten, P.O. Tjøm, W. Waluś, and I. Hamamoto, Nucl. Phys. **A559**, 100 (1993).
[52] O. Zeidan (private communication).